Published in final edited form as:
Int J Pharm. 2011 April 4; 407(1-2): 95–104. doi:10.1016/j.ijpharm.2011.01.034.

Optimization of Microdermabrasion for Controlled Removal of Stratum Corneum

Samantha N. Andrews[1], **Vladimir Zarnitsyn**[2], **Bondy Brian**[2], and **Mark R. Prausnitz**[1,2,*]

[1] Wallace H. Coulter Department of Biomedical Engineering, Georgia Institute of Technology, Atlanta, GA, USA 30332

[2] School of Chemical and Biomolecular Engineering, Georgia Institute of Technology, Atlanta, GA, USA 30332

Abstract

Microdermabrasion has been shown to increase skin permeability for transdermal drug delivery by damaging or removing skin's outer layer, stratum corneum. However, relationships between microdermabrasion parameters and effects on the stratum corneum barrier have not been developed. In this study, we determined the effect of microdermabrasion crystal flow rate, time, and suction pressure applied in both static and dynamic modes on the extent of stratum corneum removal from excised porcine skin. In addition to controlling the depth of tissue removal by microdermabrasion parameters, we also controlled the area of tissue removal by applying a metal mask patterned with 125- or 250-μm holes to selectively expose small spots of tissue to microdermabrasion. We found that the extent of stratum corneum removal depended strongly on the crystal flow rate and exposure time and only weakly on pressure or static/dynamic mode operation. Masking the skin was effective to localize stratum corneum removal to exposed sites. Overall, this study demonstrates that optimized microdermabrasion in combination with a mask can be used to selectively remove stratum corneum with three-dimensional control, which is important to translating this technique into a novel method of transdermal drug delivery.

Keywords

microdermabrasion; skin; stratum corneum; transdermal drug delivery

1. Introduction

Transdermal drug delivery involves the administration of drugs, usually from transdermal patches or topical formulations, across the skin's surface and typically into the systemic circulation (Prausnitz and Langer, 2008; Williams, 2003). This is a convenient and desirable route of delivery because skin offers a large area for delivery, therapeutics can be administered in a consistent dose that avoids the first pass effect of the liver, and needle-free delivery avoids pain and the dangers associated with hypodermic injection. Despite the ease of drug delivery using transdermal patches and ointments, the anatomy of skin only allows

*Corresponding author: Mark R. Prausnitz, School of Chemical and Biomolecular Engineering, Georgia Institute of Technology, 311 Ferst Drive, Atlanta, GA 30332-0100 USA, Ph: +1 404 894 5135, Fax: +1 404 894 2291, prausnitz@gatech.edu.

small amounts of low molecular weight, lipophilic molecules, such as estrogen and nicotine, to penetrate intact skin at therapeutic levels. This is because the main barrier to transdermal transport is the stratum corneum, which is the outer 10–15 μm layer of skin. The stratum corneum is composed of nonviable corneocytes that are surrounded by a lipid extracellular matrix. The viable epidermal and dermal layers beneath the stratum corneum typically offer much less resistance to drug transport.

To overcome the stratum corneum barrier and increase skin's permeability to hydrophilic and macromolecular compounds, the stratum corneum is often pierced for injection or removed by stripping, ablation, or abrasion (Arora et al., 2008; Banga, 2009). Devices that pierce the stratum corneum involve the use of hypodermic needles, microneedles, or jet injectors (Baxter and Mitragotri, 2006; Prausnitz, 2009). These methods lend themselves to bolus delivery and are typically either invasive, painful or both. Stratum corneum removal can be done by tape stripping, but the procedure is time consuming and requires expert technique (Fujimoto et al., 2005) Ablation utilizes energy generated by lasers or heating elements to remove the stratum corneum (Banga, 2009). Abrasion uses sandpaper or pressurized particles, such as microdermabrasion, to remove the stratum corneum (Fang et al., 2004; Fujimoto et al., 2005; Gill et al., 2009; Lee et al., 2003; Lee et al., 2006; Song et al., 2004). The advantage to using abrasion is that it is quick and painless, and that microdermabrasion is already approved by the FDA for other applications. However, current microdermabrasion equipment requires detailed characterization to determine conditions that selectively remove stratum corneum for transdermal drug delivery. Because it is the rate-limiting barrier, removal of stratum corneum by microdermabrasion can dramatically increase skin permeability, even to large molecules including proteins and vaccines (Gill et al., 2009).

Microdermabrasion is an FDA-approved cosmetic procedure that was developed in the 1980's to reduce the appearance of large pores, fine lines, wrinkles, tattoos, and superficial scars (Bhalla, 2006). Microdermabrasion damages the stratum corneum by bombarding it with abrasive particles, such as alumina or sodium chloride, under vacuum (Rajan and Grimes, 2002). Damaging stratum corneum induces an inflammatory response that results in increased collagen remodeling and proliferation, which produces the positive cosmetic results seen after microdermabrasion treatment, such as noticeably firmer skin (Freedman, 2001).

The microdermabrasion machine works by placing a handpiece on the skin, which occludes the opening of the plastic tip to create a vacuum. Upon tip occlusion, the crystals flow from the machine into the inlet port and abrade the skin. At the same time, the skin debris and used crystals are shunted back through the outlet port to the machine and collected in a waste container. This closed-loop system prevents cross-contamination between patients and exposure of medical personnel. Typically, patients undergo several sessions of microdermabrasion, depending on the severity of the skin condition, to improve the skin's appearance (Freedman, 2001; Shim et al., 2001). The procedure is noninvasive, painless, and short, and requires no down time for recovery. Typically, microdermabrasion is performed at spas or by cosmetic surgeons or dermatologists.

Several studies have shown that microdermabrasion can be used to increase transdermal delivery of low molecular weight compounds such as vitamin C (176 Da), 5-aminolaevulinic acid (130 Da), 5-Fluorouracil (467 Da), lidocaine (234 Da) and estradiol (272 Da) (Fang et al., 2004; Fujimoto et al., 2005; Herndon, 2004; Lee et al., 2003; Lee et al., 2006). We also showed in a previous study that microdermabrasion can be used to completely remove the stratum corneum in humans and monkeys and demonstrated increased skin permeability to fluorescein (332 Da) and a model viral vaccine (Modified Vaccina Ankara) (Gill et al.,

2009). Abrasion can also be used in conjunction with a mask to minimize and control the area of abrasion (Herndon, 2004).

Building off these previous findings, this study sought to develop a microdermabrasion method that offers three-dimensional control over stratum corneum removal, which should provide improved control over transdermal drug delivery. Control over depth of abrasion, and the ability to completely remove stratum corneum without damaging deeper tissue, was pursued through a detailed analysis of the effects of microdermabrasion crystal flow rate, time, suction pressure, and handpiece movement. To control the area of abrasion, we designed a mask to cover the skin and allow microdermabrasion to occur only through small holes in the mask, thereby localizing tissue removal to specific locations. In this way, we could control the size of holes made in the skin by microdermabrasion in all three dimensions.

2. Materials and methods

2.1. Microdermabrasion Procedure

Microdermabrasion experiments were conducted on excised adult feeder porcine (2–9 month old, average weight 32 kg) dorsal skin (Pel-freeze Biologicals, Rogers, AR) using a Gold Series MegaPeel microdermabrasion machine (DermaMed USA, Lenni, PA) with the gold handpiece assembly. Pig skin was obtained with approval from the Georgia Tech Institutional Animal Care and Use Committee. The skin was stored at −70 °C prior to use. Before the experiments were conducted, subcutaneous fat was removed from the skin using a scalpel (Fisher Scientific, Fair Lawn, NJ) and the hair was carefully removed using surgical prep razors (Medex Supply, Monsey, NY) without damaging the skin.

A picture of a microdermabrasion machine tip and the alumina crystals are shown in Figure 1A and B, respectively. The experiments were carried out using two different abrasion modes: static and dynamic. For the static mode, the machine handpiece remained stationary on the skin for 6 s. For the dynamic mode, it was moved along the skin for 10 passes at a rate of 1 pass/s. The dynamic mode experiments were carried out by first isolating the area of abrasion with a rectangular foam adhesive (Avery Dennison, Painesville, OH) having inner dimensions measuring 41 mm long and 15 mm wide and sliding the probe back and forth within this area.

For both abrasion modes, the effect of crystal flow rate and suction pressure were examined. The crystal flow rate was varied from the minimum value (corresponding to a setting of 9 turns of the crystal flow rate knob on the microdermabrasion machine) to the maximum value (corresponding to a setting of 0 turns of the crystal flow rate knob). As discussed in the Appendix, we determined this range of crystal flow rates to span 8.9×10^2 to 2.2×10^5 particles/s or <0.01 to 0.80 g/s of particles. The suction pressure was also varied from −30 kPa to −60 kPa. All experiments were carried out in triplicate.

We also studied the effect of time on depth of skin abrasion as a function of the crystal flow rate and pressure for the static and dynamic abrasion modes using porcine skin. For the static mode, the crystal flow rate was fixed at 4 turns and the time points studied were 3, 20, and 45 s at suction pressures of −30, −40, and −50 kPa. For the dynamic mode, the flow rate was set to 4.5 turns and the suction pressures examined were −25 and −45 kPa for 1, 10, and 50 passes. All experiments were carried out in triplicate.

At the conclusion of each experiment, an 8 mm skin biopsy was taken with a biopsy punch (Miltex Inc, York, PA), embedded in Optimal Cutting Temperature compound (Sakura Finetek, Torrance, CA) and frozen in dry ice for histological analysis. The skin was

sectioned using a Leica 3050S cryostat (Leica Microsystems, Wetzlar, Germany) at a thickness of 10 μm, stained with routine hematoxylin and eosin (H&E), and imaged using a Nikon 600E microscope (Nikon, Tokyo, Japan) and Qcapture software (Q Imaging, Pleasanton, CA).

2.2. Abrasion Depth Quantification

The depth of abrasion was quantified by assigning values to indicate the degree of stratum corneum removal. For the experiments in which the time was held constant, 0 indicated stratum corneum not removed, 0.5 represented partial stratum corneum removal, and 1 corresponded to complete stratum corneum removal. For the experiments in which the time was varied, 0 was assigned for stratum corneum not removed, 0.5 for partial stratum corneum removal, 1 for complete stratum corneum removal, and 1.5 for viable epidermis removal. For each condition, 20 histological sections from 3 replicate experiments were examined and scored. Average scores are reported in the figures.

2.3. Microdermabrasion Using a Skin Mask

To control the area of abrasion, two masks with an array of holes (125 μm or 250 μm diameter) were designed using AutoCAD software (Autodesk, San Rafael, CA) and fabricated out of stainless steel (75 μm thickness, Trinity Brand Industries, Countryside, IL). The pattern was cut into the metal using an infrared laser (Resonetics Maestro, Nashua, NH) and the masks were manually cleaned with detergent (Contrex, Decon Labs, King of Prussia, PA) to de-grease the surface and remove slag and oxides deposited during laser cutting, which was followed by thorough rinsing in running deionized water. To deburr and clean edges, the masks were electropolished in SS Electropolish solution (E972, ESMA, South Holland, IL). The process was carried out in an electropolisher (E399-100, ESMA) using 6 V for 15 min. After electropolishing, the masks were cleaned by dipping alternately three times in de-ionized water and 25% nitric acid (Fisher Scientific) for 30 s each. This was followed by another washing step in hot running water and a final wash in running de-ionized water. Due to the electropolishing process, the thickness of the masks was reduced to 50 μm. Masks were dried using compressed nitrogen.

For the microdermabrasion experiments, the mask was adhered to the center of a rectangular foam adhesive (Avery Dennison, Painesville, OH) and attached to the skin. A picture of the mask and a schematic of the skin after abrasion are shown in Figures 1C and D, respectively. In experiments using the mask, excised porcine cadaver skin was abraded at a pressure of −50 kPa at the maximum crystal flow rate (0 turns) for 30, 45, 60, 90, and 120 s to determine the optimal removal setting. A negative control experiment was also conducted using the conditions of −50 kPa at minimal crystal flow rate (9 turns) for 60 s. The site of abrasion was revealed by staining with green dye (McCormick & Co, Hunt Valley, MD). After the experiment, the area of abrasion was excised and frozen for histological examination using the same protocol as mentioned in the previous section.

2.4. Statistical Analysis

Statistical analysis was carried out using Minitab software (Minitab Inc., State College, PA). A two-way ANOVA was used for statistical evaluations. The p value was set to 0.05.

3. Results

3.1. Control Over Depth of Microdermabrasion by Optimization of Operating Parameters

To control depth of microdermabrasion, this study sought to understand how the primary microdermabrasion operating parameters of crystal flow rate, suction pressure, time, and handpiece movement affected stratum corneum removal.

3.1.1. Static Mode—For the static mode, the microdermabrasion handpiece was held stationary against the skin for 6 s at the specified conditions. The skin was abraded at suction pressures of −30, −40, −50, and −60 kPa at 1, 4, and 9 turns of the crystal flow rate knob. A setting of 1 turn of the crystal flow rate knob corresponded to a flow rate of ~2×10^5 particles/s or ~0.60 g/s at an average velocity of ~1.5 m/s. A setting of 4 turns corresponded to a flow rate of ~1×10^5 particles/s or ~0.3 g/s at an average velocity of ~2 m/s. The flow rate was too low for accurate quantification at a setting of 9 turns, but the average velocity was found to be ~3 m/s. See the Appendix for more information about these measurements and calculations.

For reference, Figure 2 shows an intact piece of skin without microdermabrasion treatment. The full thickness of red-stained stratum corneum is present, the blue-stained nuclei of the viable epidermis are seen below, and the pink-stained dermis is deeper still.

Figure 3 and 4 show the results of the static mode experiments. Figure 3 presents histological images of representative skin sections after microdermabrasion and Figure 4 quantifies these data by scoring the extent of stratum corneum removal and averaging among replicates. As shown in the left column of Figure 3, microdermabrasion at the most aggressive crystal flow rate (1 turn) completely removed the stratum corneum from skin abraded at pressures of −50 and −60 kPa and partially removed at pressures of −30 and −40 kPa. Partial stratum corneum removal is indicated by bits of stratum corneum still adherent to the skin surface. The viable epidermis remained intact under these conditions, except at −60 kPa, which had small focal areas of deeper tissue removal.

The intermediate crystal flow rate (4 turns) resulted in partial stratum corneum removal at all suction pressures (Figure 3, center column). For all suction pressures at the lowest crystal flow rate (9 turns), the stratum corneum remained intact (Figure 3, right column). At 9 turns, the greatest contribution to possible tissue removal appeared to be suction pressure, because there is very little crystal flow.

Overall, as the crystal flow rate increased, the degree of stratum corneum removed increased for all pressures (Figure 4, two-way ANOVA, $P < 0.05$). Pressure did not significantly affect stratum corneum removal (Figure 4, two-way ANOVA, $P > 0.05$).

We also sought to evaluate the effect of time on the amount of stratum corneum removal. For the static mode, the skin was abraded at suction pressures of −30, −40, and −50 kPa for 3, 20, and 45 s at 4 turns of the crystal flow rate knob. The histological results for the static mode are shown in Figure 5. Quantification of the amount of stratum corneum removed is presented in Figure 6. At suction pressures of −30 and −40 kPa at 3 s the stratum corneum remained intact (Figure 5 left column). For a suction pressure of −50 kPa at 3 s, the stratum corneum was removed and the viable epidermis remained intact. However, at 20 and 45 s stratum corneum and viable epidermis were removed at all pressures tested (Figure 5 center and right columns). Overall, time had a significant effect on tissue removal (Figure 6, two-way ANOVA, $P < 0.05$), but the effects of pressure were not significant (Figure 6, two-way ANOVA, $P > 0.05$). These results demonstrate the importance of exposure time on the depth of abrasion, in addition to the important role of crystal flow rate demonstrated above.

3.1.2. Dynamic Mode—For the dynamic mode experiments, the skin was abraded at the same crystal flow rates and suction pressures as the static mode, but the microdermabrasion handpiece was moved across the skin for 10 passes at a rate of 1 pass/s. Figure 7 presents histological images of representative skin sections after microdermabrasion and Figure 8 quantifies these data. At the most aggressive crystal flow rate (1 turn), the stratum corneum was completely removed for all pressures and the viable epidermis remained intact (Figure

7, left column). At 4 turns of the crystal flow rate knob, the stratum corneum was partially removed for all pressures (Figure 7, center column). At 9 turns, the stratum corneum remained intact on the skin (Figure 7, right column). Similar to the static mode, increasing the crystal flow rate significantly increased the amount of stratum corneum removal (Figure 7, two-way ANOVA, $P < 0.05$), whereas suction pressure did not have a significant effect (Figure 8, two-way ANOVA, $P > 0.05$).

For the dynamic mode time experiments, the number of passes was set at 1, 10 or 50 passes, which was performed using suction pressures of −25 and −45 kPa at 4.5 turns. The histological images of skin and quantitative analysis of the degree of stratum corneum removal is shown in Figures 9 and 10, respectively. For both pressures at 1 pass, the stratum corneum remained intact (Figure 9 right column). At the 10 passes, the skin treated at −25 kPa had partial stratum corneum removal and skin abraded at −45 kPa had complete stratum corneum removal (Figure 9 middle column). At 50 passes, both samples had complete stratum corneum removal (Figure 9 left column). For all times and pressures the viable epidermis remained intact. Through quantitative analysis of these experiments, however, neither time (Figure 10, two-way ANOVA, $P = 0.07$) nor pressure (Figure 10, two-way ANOVA, $P > 0.05$) was found to have a statistically significant effect. This lack of statistical significance is possibly due to the small sample size, because only two pressures were examined.

3.2. Control Over Area of Microdermabrasion By Using a Mask

We have shown above that optimization of microdermabrasion parameters can control the depth of stratum corneum removal. Next, we wanted to control the area of removal and thereby achieve three-dimensional control over pore formation. To accomplish this, we designed a mask to partially cover the skin's surface and, in that way, only expose selected spots on the skin to microdermabrasion (Figures 1C and 1D).

3.2.1. Mask Design—In the experiments to optimize microdermabrasion conditions presented above, a single, large area of skin (i.e., many cm^2) was abraded. Abrading such a large area may be cosmetically unacceptable, take too long to heal, and present increased risk of infection. For that reason, we now introduce the use of a mask to make an array of microscopically small pores. While we wanted the holes in the mask to be as small as possible, they also needed to be large enough to permit the microdermabrasion crystals to flow through and contact the skin. Larger holes also reduced the chances of occlusion due to particle clogging. By measuring 100 particles using scanning electron microscopy, we determined the average particle long-axis to be 203 μm ± 59 μm long and the average short-axis to be 141 μm ± 86 μm long. We therefore selected a mask hole diameter of 125 μm, which allowed smaller particles to impact skin and prevented larger particles from causing deep abrasion. Center-to-center spacing between the holes was set at 500 μm.

Mask thickness was also a concern, because a thicker mask would increase the distance between the skin and the crystal flow from the machine, making particle entry into the hole to contact the skin more difficult. However, a thinner mask might be excessively damaged during the abrasion process (i.e., the crystals not only abrade the skin, but also abrade the mask). Given these constraints, we selected a mask thickness of 50 μm. Made out of stainless steel, this mask provided sufficient durability, but was also sufficiently flexible to conform to the skin surface.

Lastly, we found that the presence of hairs was an important factor because hairs impeded good contact between the mask and the skin. Moreover, the hairs themselves served as masks that blocked microdermabrasion crystals from contacting the skin. The very thick hairs present on the porcine skin used in this study needed to be shaved for good results.

3.2.2 Microdermabrasion Using a Mask—The effect of the mask during microdermabrasion was assessed using the static abrasion mode at a suction pressure of −50 kPa for 30, 45, 60, 90, and 120 s at the maximum crystal flow rate (0 turns). For all times, complete removal of stratum corneum was observed and the viable epidermis remained intact, as shown in Figure 11. We used these relatively aggressive microdermabrasion conditions because of the expectation that the presence of the mask would (i) reduce the effectiveness of microdermabrasion and (ii) provide a possible self-limiting effect due to the inability of microdermabrasion crystals to penetrate deeply through the narrow holes in the mask.

Histological examination presented in Figures 11A–11C shows representative pores formed in the skin. Their depth spans the full thickness of the stratum corneum, but without damaging viable epidermis. The average width of the pores was 95 ± 25 μm, based on measurement of histological sections of 10 pores from 3 different skin samples. This pore size is somewhat smaller than the mask hole size probably because microdermabrasion crystals, which abrade the skin by impacting it primarily at an angle, have difficulty abrading skin along the edges of the mask hole. As a negative control experiment to determine the role of suction alone on tissue removal, we also exposed skin in the static abrasion mode to a suction pressure of −50 kPa for 60 at the minimum crystal flow rate (9 turns). This application of suction with minimal crystal flow was ineffective to remove tissue (data not shown).

Figure 11F shows a lower-magnification, en face view of the skin surface after microdermabrasion at the same conditions used in Figure 11B. Staining with a green dye shows pore formation in the skin following the pattern of the mask (Figure 1C). Closer examination of the pores shows that the green-stained spots have an average diameter of 118 ± 39 μm, based on measurement of 10 pores from 3 different skin samples. Some of the pore diameters were larger than the mask hole diameter and the pore size shown by histology, possibly due to lateral diffusion of dye within the skin.

In Figure 11D, microdermabrasion was carried out using a mask with 250 μm diameter holes. This larger mask hole size led to removal of stratum corneum as well as much of the viable epidermis. This shows that mask hole size not only affects the area of tissue removal but also affects the depth of tissue removal. In Figure 11E, skin was microdermabraded at the same condition as the skin in Figure 11A, but without any mask. In this case, not only was the area of skin abrasion large, but the full epidermis was removed. This further shows that the mask not only limits the area of abrasion, but also influences the depth. The observation that microdermabrasion with the 125-μm mask was independent of exposure time over the range of 30–120 s studied here further suggests a self-limiting feature enabled by the mask. We hypothesize that microdermabrasion crystals are only able to penetrate to a limited depth into the mask holes and this limits how much tissue they can remove. Moreover, we observed the holes to become clogged with microdermabrasion particles over time. This may close off holes and thereby stop further skin abrasion after a period of time. More work is needed to fully understand this self-limiting feature.

4. Discussion

This study showed for the first time that controlled microdermabrasion using optimized operating parameters in combination with a mask enabled three-dimensional control of tissue removal that selectively and completely removed small spots of stratum corneum without removing the viable epidermis. Selective removal of stratum corneum is important because damage to the viable epidermis causes trauma to living tissue that could be painful, take longer to heal, and generate cosmetically undesirable appearance. Complete removal of

stratum corneum is important because this is needed to eliminate the primary barrier to drug delivery.

We studied the effect of crystal flow rate, suction pressure, exposure time, and handpiece movement on stratum corneum removal and found that crystal flow rate and exposure time had the greatest impact on stratum corneum removal. Over the range of conditions studied, suction pressure had no significant effect. Both static and dynamic handpiece movements were effective. We believe that the crystal flow rate was important because the crystals shear and tear the stratum corneum and, therefore, the number of times crystals impact the skin should correlate with the degree of tissue removal (Bhalla, 2006). The exposure time was also an important parameter for similar reasons; increased exposure time increased the number of crystal-skin impacts. The suction pressure, in contrast, had no significant effect on the crystal flow rate or velocity (see Appendix) and, correspondingly, no significant effect on tissue removal. We believe that the suction pressure serves to help remove skin debris and crystals from the skin surface and into the refuse canister of the microdermabrasion machine. In this way, suction is important to proper function of the microdermabrasion method, but it does not control the tissue removal process.

The importance of crystals in microdermabrasion has been shown in a previous study in which inclusion of crystals increased the expression of proteins needed for dermal remodeling, which is the primary purpose of conventional cosmetic microdermabrasion, as compared to suction pressure alone (Karimipour DJ, 2006). However, suction pressure alone (i.e., without crystals) has been shown to remove stratum corneum at pressures of −20 to −40 kPa when the skin was exposed for 24 s (Pedersen and Jemec, 2006). Although similar suction pressures were applied in this study for up to similar periods of time (≤ 45 s static mode and ≤ 50 s dynamic mode), no stratum corneum removal was observed without significant crystal flow. While the different exposure times may play a role, the fact that our study used pig skin in vitro and the study that removed stratum corneum with suction alone used human skin in vivo may also be relevant. Consistent with this expectation, a previous study with human skin in vivo found that static mode microdermabrasion at conditions that removed stratum corneum also caused microblisters (i.e., localized separation of epidermis from the underlying dermis) (Gill et al., 2009) but this was not observed in the present study using pig skin in vitro. This suggests that human skin in vivo may be more susceptible to suction-induced damage than pig skin in vitro.

Both handpiece abrasion modes resulted in selective stratum corneum removal, however the dynamic mode appears to offer advantages (in addition to the lack of microblisters found previously (Gill et al., 2009)). For example, stratum corneum removal in the static experiments was not as uniform as in the dynamic experiments and the area of tissue removal is limited to that of the microdermabrasion tip (0.4 cm^2). The dynamic mode enabled a larger area of removal (3 cm^2 in this study) and the results were more consistent. Additionally, the dynamic mode is typically used in the clinical setting for cosmetic microdermabrasion.

Use of a mask in combination with microdermabrasion limited both the area and depth of tissue removal. As discussed above, generating an array of small pores using a mask may be preferable from a safety, cosmetic and patient preference perspective compared to removing stratum corneum from large, continuous areas of skin. By selecting a mask hole diameter that was slightly smaller than the size of the crystal particles, the mask further served to limit the depth of tissue remove, such that 125-μm holes provided a self-limiting feature that achieved selective removal of stratum corneum independent of exposure time and using aggressive microdermabrasion operating parameters. In this way, the use of a mask was critically important, and arguably more important than the microdermabrasion operating

parameters, to enable three-dimensional control over pore formation on the micron scale localized to the stratum corneum.

The pores generated in this study were on the order of 10 μm deep and 100 μm wide. The width of these pores is similar to those created by thermal ablation and piercing with microneedles (Arora et al., 2008; Banga, 2009; Prausnitz, 2009), both of which have been well tolerated in numerous human studies and both of which enable delivery of a broad range of compounds, including large hydrophilic molecules and vaccines. In separate work from our laboratory, microdermabrasion under the conditions used in this study has been shown to increase permeability of human cadaver skin to macromolecules in vitro and to effectively administer insulin to diabetic rats (data not shown). This suggests that the holes made by microdermabrasion should likewise be well tolerated and effective for drug delivery. However, the pores made in the present study are much less deep that those made by thermal ablation or using microneedles, which may make them still better tolerated by patients.

Comparing more broadly to other methods of transdermal drug delivery, there are several additional expected advantages to using microdermabrasion to increase skin permeability. First, microdermabrasion is a well-established clinical technique used routinely for cosmetic applications that is safe, minimally invasive, requires no down time, and does not leave scars (Lee et al., 2006). Competing methods that disrupt stratum corneum structure on the molecular scale, such as chemical enhancers, ultrasound, and iontophoresis, are generally limited to delivering low molecular weight molecules and small macromolecules, because the stratum corneum is left largely intact (Prausnitz and Langer, 2008; Williams, 2003). Methods that pierce the stratum corneum, such as microneedles, jet injectors, and hypodermic needles, can cause pain, require regulated disposal, and may require professional help for administration. Other methods that completely remove the stratum corneum, such as tape stripping and laser ablation, are generally regarded as impractical for widespread use due to cost and reproducibility (Fang et al., 2004; Fujimoto et al., 2005). In contrast to these other methods, microdermabrasion has the advantage of being quick, painless, reproducible and able to generate micron-scale pores that selectively breach the stratum corneum barrier layer.

5. Conclusion

This study showed that controlled microdermabrasion can be used to selectively remove stratum corneum in a targeted fashion without removing viable epidermis. Crystal flow rate and exposure time were the most important parameters in controlling stratum corneum removal, whereas suction pressure and handpiece movement had lesser effects. Notably, this study added the use of a mask to limit tissue removal to an array of micron-scale pores rather than one large region of stratum corneum removal. We found that the mask also influenced the depth of tissue removal; the 125 μm-hole mask limited tissue removal to the stratum corneum in a self-limiting manner independent of exposure time to microdermabrasion. In this way, precise control over pore geometry was achieved such that arrays of pores on the order of 100 μm in diameter and 10 μm in depth (i.e., the thickness of stratum corneum) were demonstrated. Because stratum corneum is the skin's main permeability barrier, controlled microdermabrasion offers a novel approach to increasing rates of transdermal drug delivery. The established clinical safety record and the non-invasive nature of microdermabrasion suggest that this approach should be safe, painless, cosmetically acceptable and effective to deliver a broad range of pharmaceutical compounds.

Supplementary Material

Refer to Web version on PubMed Central for supplementary material.

Acknowledgments

We thank Dr. Harvinder Gill for his advice and guidance for this project, Dr. Leslie Coburn for use of the high speed digital camera and software, Dr. Jonathan Colton for his advice interpreting the data, and Donna Bondy for administrative support. This work was carried out in the Center for Drug Design, Development and Delivery and the Institute for Bioengineering and Bioscience at Georgia Tech with financial support in part from the National Institutes of Health.

Abbreviations

H&E hematoxylin and eosin

References

Arora A, Prausnitz MR, Mitragotri S. Micro-scale devices for transdermal drug delivery. Int J Pharm 2008;364:227–236. [PubMed: 18805472]

Banga AK. Microporation applications for enhancing drug delivery. Expert Opin on Drug Deliv 2009;6:343–354.

Baxter J, Mitragotri S. Needle-free liquid jet injections: mechanisms and applications. Expert Rev of Med Devices 2006;3:565–574. [PubMed: 17064242]

Bhalla M, Thami Gurvinder P. Microdermabrasion: Reappraisal and Brief Review of Literature. Am Soc of Dermatol Surg 2006;32:809–814.

Fang JY, Lee WR, Shen SC, Fang YP, Hu CH. Enhancement of topical 5-aminolaevulinic acid delivery by erbium : YAG laser and microdermabrasion: a comparison with iontophoresis and electroporation. Br J Dermatol 2004;151:132–140. [PubMed: 15270882]

Freedman B, Rueda-Pedraza Eugenia, Waddell Sharon. The epidermal and dermal changes associated with microdermabrasion. Chem Pharm Bull 2001;27:1031–1034.

Fujimoto T, Shirakami K, Tojo K. Effect of microdermabrasion on barrier capacity of stratum corneum. Chem Pharm Bull 2005;53:1014–1016. [PubMed: 16079538]

Gill HS, Andrews SN, Sakthivel SK, Fedanov A, Williams IR, Garber DA, Priddy FH, Yellin S, Feinberg MB, Staprans SI, Prausnitz MR. Selective removal of stratum corneum by microdermabrasion to increase skin permeability. Eur J Pharm Sci 2009;38:95–103. [PubMed: 19559791]

Hendriks FM, Brokken D, Oomens CWJ, Baaijens FPT. Influence of hydration and experimental length scale on the mechanical response of human skin in vivo, using optical coherence tomography. Skin Res and Tech 2004;10:231–241.

Herndon T, Gonzalez Salvador, Gowrishankar TR, Anderson R, Weaver James. Transdermal microconduits by microscission for drug delivery and sample acquisition. Biomed Central 2004;2:11.

Karimipour DJ, KS, Johnson TM, Orringer JS, Hamilton T, Hammerberg C, Voorhees JJ, Fisher G. Microdermabrasion with and without aluminum oxide crystal abrasion: A comparative molecular analysis of dermal remodeling. J Am Acad of Derm 2006;54:405–410. [PubMed: 16488289]

Lee WR, Shen SC, Wang KH, Hu CH, Fang JY. Lasers and microdermabrasion enhance and control topical delivery of vitamin C. J Invest Dermatol 2003;121:1118–1125. [PubMed: 14708614]

Lee WR, Tsai RY, Fang CL, Liu CJ, Hu CH, Fang JY. Microdermabrasion as a novel tool to enhance drug delivery via the skin: An animal study. Dermatol Surg 2006;32:1013–1022. [PubMed: 16918563]

Pedersen L, Jemec GBE. Mechanical properties and barrier function of healthy human skin. Acta Dermatol Venereol 2006;86:308–311.

Prausnitz MR, Langer R. Transdermal drug delivery. Nat Biotechnol 2008;26:1261–1268. [PubMed: 18997767]

Prausnitz MR, Mikszta JA, Cormier M, Andrianov AK. Microneedle-based vaccines. Curr Top Microbiol Immunol 2009;333:369–393. [PubMed: 19768415]

Rajan P, Grimes PE. Skin barrier changes induced by aluminum oxide and sodium chloride microdermabrasion. Dermatol Surg 2002;28:390–393. [PubMed: 12030870]

Shim EK, Barnette D, Hughes K, Greenway HT. Microdermabrasion: A clinical and histopathologic study. Dermatol Surg 2001;27:524–530. [PubMed: 11442587]

Song JY, Kang HA, Kim MY, Park YM, Kim HO. Damage and recovery of skin barrier function after glycolic acid chemical peeling and crystal microdermabrasion. Dermatol Surg 2004;30:390–394. [PubMed: 15008867]

Williams, A. Transdermal and Topical Drug Delivery. 1. Pharmaceutical Press; London: 2003.

APPENDIX

A1. Introduction

In this study, we used the DermaMed Goldseries microdermabrasion device. Because the manufacturer provides little information to characterize the device's operating parameters, and not much additional information exists in the literature, we carried out a detailed characterization in order to better understand device performance and interpret our data.

The device has two settings that can be controlled by the operator: "vacuum," which is the suction pressure measured in gauge units of kPa, and "crystal," which is the crystal flow rate measured in relative units ranging from 0 (highest flow rate) to 9 (lowest flow rate) knob turns. We first sought to quantify crystal flow rate in absolute units (i.e., particles per second and mass per second) by directly measuring the mass moving through the machine. We next determined particle velocity as a function of operating conditions using video microscopy.

A2. Materials and methods

The crystal mass flow rate was determined as a function of suction pressure at −30, −40, −50, and −60 kPa and crystal flow rates corresponding to 0, 1, 3, 4, 6, and 9 knob turns for 3 to 60 s. Zero knob turns is the maximum valve opening, whereas at nine turns the valve is almost closed. The absolute crystal flow rate at each turn has not been previously characterized by the manufacturer. Our experiments were carried out by weighing the microdermabrasion device waste container prior to the experiment with a BP 2100 Sartorius balance (Sartorius Group, Goettingen, Germany). The device was then set to a specified pressure and crystal flow rate, and porcine skin was abraded using the static mode. The final weight of the waste container was measured at the conclusion of the experiment, and the mass of the crystals consumed was determined by subtracting the final canister mass from the initial mass. Measurements at each setting were carried out in triplicate.

To convert mass flow rate into particle flow rate, we used the following equation: $P = M/m$, where P is particle flow rate (particles/s), M is mass flow rate (g/s), and m is the average particle mass, which was determined to be 3.0 ± 0.21 μg per particle. The average particles mass was estimated by counting the number of particles in a 2.2 mg sample of particles by microscopic imaging and averaging the result of three replicate measurements.

The velocity of the particles was measured using a Phantom B4.2 high speed camera (Vision Research, Wayne, NJ). The camera imaged the particles in the handpiece tip at pressures of −30, −40, and −50 kPa and at crystal flow rates corresponding to 0, 3, 6, and 9 turns. Particle velocity was also measured for −60 kPa for 1 and 4 turns. The videos were captured using the Phantom Camera Control software (Vision Research) and analyzed using Image J

(National Institutes of Health, Bethesda, MD), QuickTime (Apple, Cupertino, CA), Microsoft Office Picture Manager (Microsoft, Redmond, WA), and Digitizing Tools Software (Hendricks Lab,Chapel Hill, NC) (Hendriks et al., 2004). Each video was recorded for 0.54 s at a capture rate of 10,000 frames/s. Four videos of each setting were recorded and, for each video, 20 particles were tracked over 10 frames to determine the velocity by directly measuring the distance traveled per time increment.

A3. Results

A.3.1 Crystal Mass and Particle Flow Rate

The crystal mass and particle flow rates were determined as a function of crystal flow rate knob turns and as a function of pressure. Figure A1A shows mass flow rate over time at crystal knob settings of 1, 3, 6, and 9 turns at a suction pressure of −50 kPa. These data show that (i) mass flow rate did not significantly change with time at all crystal flow rate knob turns (two-way ANOVA, $P \geq 0.05$) and (ii) mass flow rate increased with decreasing crystal flow rate knob turns (two-way ANOVA, $P < 0.05$). In Figure A1B, mass flow rate is shown over time as a function of suction pressure. Over the range of conditions studied, suction pressure did not significantly affect the crystal mass flow rate (two-way ANOVA, $P > 0.05$). Mass flow rate data are also presented as the number of particles per second.

Guided by the observation that crystal flow rate is generally independent of time, we determined mass flow rates over a broader range of suction pressures and crystal flow rates, which is shown in Figure A2. These data further demonstrate that crystal mass flow rate depends on the crystal knob setting (two-way ANOVA, $P < 0.05$) and does not depend on suction pressure (two-way ANOVA, $P > 0.05$). Over the range of conditions used in this study (which generally spans the range of conditions enabled by the microdermabrasion machine), crystal mass flow rates varied up to more than 0.7 g/s and 2×10^6 particles/s.

A.3.2 Crystal Velocity

Average crystal particle velocity was measured as a function of crystal flow rate and suction pressure, as shown in Figure A3. These data show that velocity varied with crystal flow rate (two-way ANOVA, $P < 0.05$) but did not depend on suction pressure (two-way ANOVA, $P > 0.05$). More specifically, particle velocity was generally slower at higher particle flow rates (i.e., smaller number of crystal flow rate knob turns). Particle velocities ranged from approximately 1 m/s to 3.5 m/s under the conditions used in this study (which generally span the range of conditions enabled by the microdermabrasion machine).

Closer examination of the video images used to determine particle velocity shows that the slower particle speed at higher particle flow rates appears to be due to the higher density of particles in the handpiece, which results in larger numbers of particle-particle collisions, thus reducing the particles' speed. This can be seen by comparing Supplementary Video 1, which shows few particle collisions at a setting of 9 crystal knob turns and −30 kPa suction pressure, and Supplementary Video 2, which shows many more particle collisions at a setting of 1 crystal knob turn and −30 kPa suction pressure. These videos also show evidence of particles breaking apart upon collision, which increases particle number and decreases particle size.

A4. Discussion and Conclusions

This study provides the first detailed characterization of the physical operating parameters of this or, to our knowledge, any microdermabrasion machine. The mass flow rate, particle flow rate, and particle velocity were determined over most of the range of operating conditions enabled by the machine. The mass flow rate and particle flow rate increased as

the opening of the crystal flow rate valve increased (i.e., at decreasing crystal flow rate knob turns). Mass flow rates ranged up to more than 0.7 g/s and particle flow rates ranged up to more than 2×10^6 particles/s. Crystal flow rate was found to be independent of time and suction pressure. Particle velocity was shown to vary between 1.0 cm/s and 3.5 cm/s and to decrease at increasing crystal flow rate due primarily to increased number of particle-particle collisions.

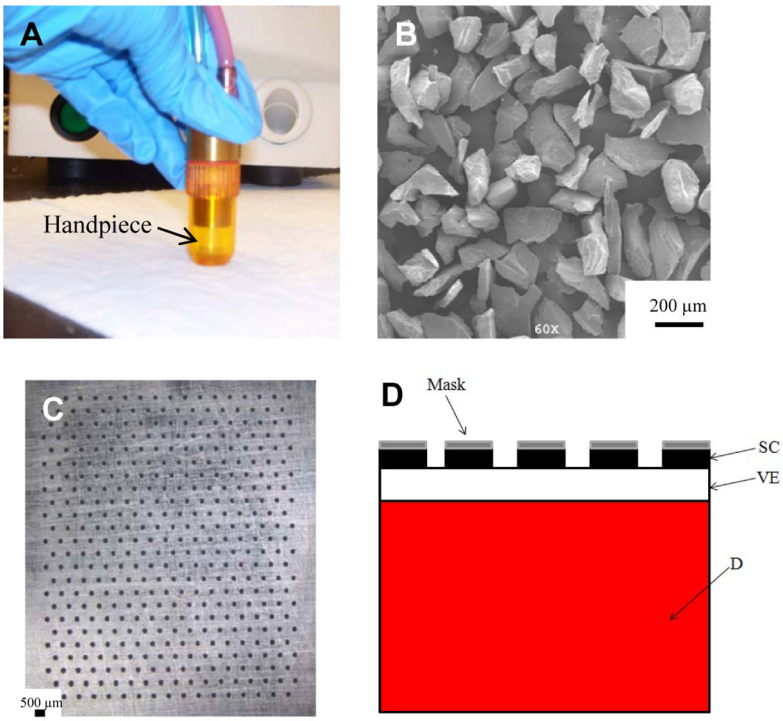

Figure 1.

Microdermabrasion device and mask. (A) Microdermabrasion machine handpiece and (B) the alumina abrasion crystals (~100 μm in diameter). (C) Stainless steel mask with 408 holes (125 μm diameter). (D) Schematic diagram of the skin after abrasion with the mask, where the stratum corneum is selectively removed and the underlying layers are intact. SC = stratum corneum, VE = viable epidermis, and D = dermis.

Figure 2.
Histological section of intact porcine cadaver skin stained with H&E. The stratum corneum appears on top with a red stain. Viable epidermis is immediately below with characteristic blue staining of epidermal cell nuclei. The pink-stained dermis is below that.

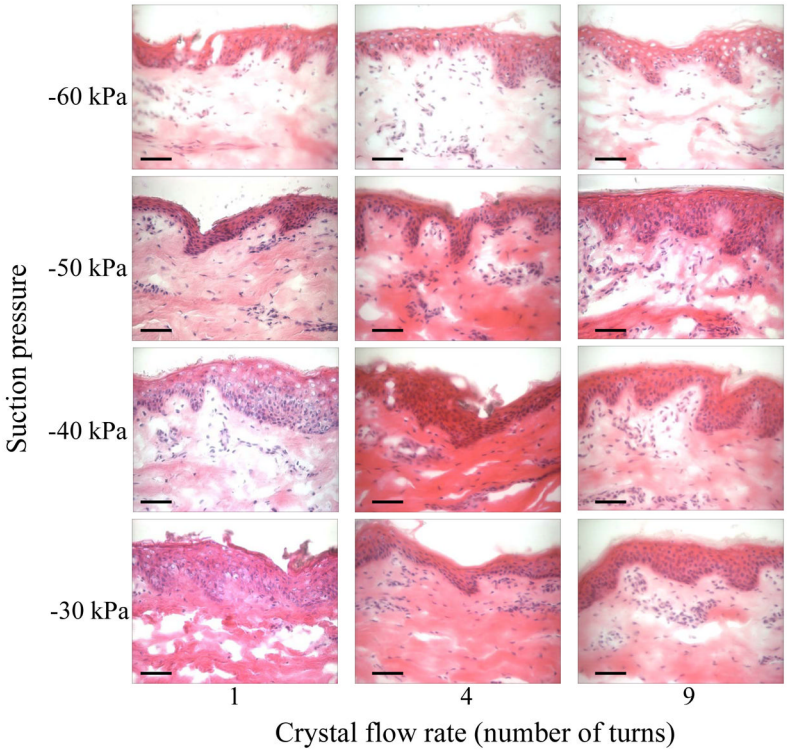

Figure 3.
Skin abraded using static mode microdermabrasion at −30, −40, −50, and −60 kPa suction pressure for 1, 4, and 9 turns of the crystal flow rate knob applied for 6 s. Crystal flow rate scales inversely with the number of knob turns, such that 9 turns corresponds to the smallest crystal flow rate (see Appendix for more information). Representative H&E-stained sections of porcine cadaver skin are shown. Scale bar = 50 μm.

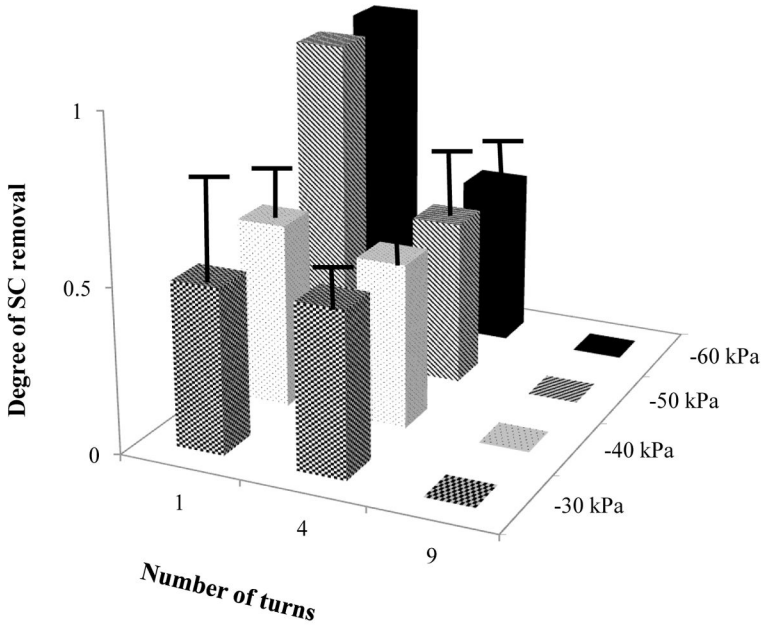

Figure 4.

Degree of stratum corneum removal during static mode microdermabrasion at −30, 40, −50, and −60 kPa suction pressure at 1, 4, and 9 turns of the crystal flow rate knob applied for 6 s. Complete stratum corneum removal = 1, partial stratum corneum removal = 0.5, and stratum corneum not removed = 0. Data represent the average of three replicate measurements ± standard deviation.

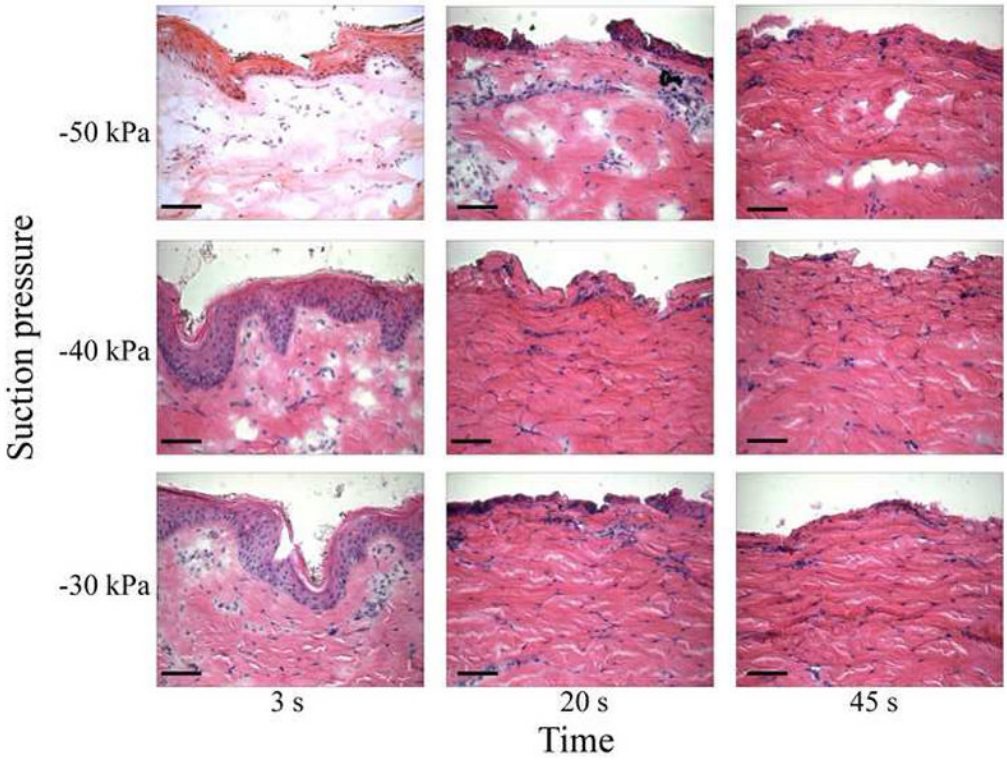

Figure 5.
Skin abraded using the static mode at −30, −40, and −50 kPa suction pressure at 4 turns of the crystal flow knob applied for 3, 20, and 45 s. Representative H&E-stained sections of porcine cadaver skin are shown. Scale bar = 50 μm.

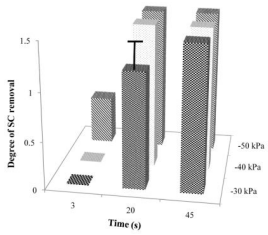

Figure 6.

Degree of stratum corneum removal during static mode microdermabrasion at −30, 40, and −50 kPa suction pressure at 4 turns of the crystal flow knob applied for 3, 20, and 45 s. Viable epidermis removal=1.5, complete stratum corneum removal = 1, partial stratum corneum removal = 0.5, and stratum corneum not removed = 0. Data represent the average of three replicate measurements ± standard deviation.

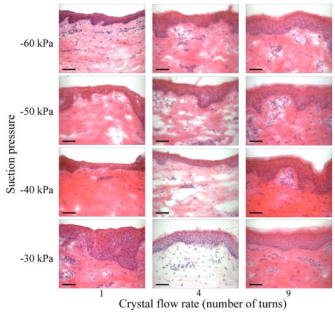

Figure 7.

Skin abraded using dynamic mode microdermabrasion at −30, −40, −50, and −60 kPa suction pressure for 1, 4, and 9 turns of the crystal flow rate knob applied for 10 passes. Representative H&E-stained sections of porcine cadaver skin are shown. Scale bar = 50 μm.

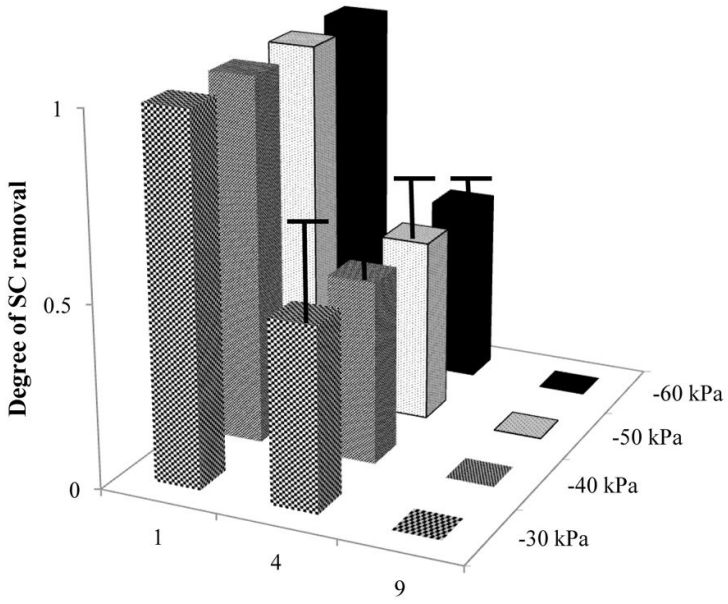

Figure 8.

Degree of stratum corneum removal during dynamic mode microdermabrasion at −30, 40, −50, and −60 kPa suction pressure at 1, 4, and 9 turns of the crystal flow rate knob applied for 10 passes. Complete stratum corneum removal = 1, partial stratum corneum removal = 0.5, and stratum corneum not removed = 0. Data represent the average of three replicate measurements ± standard deviation.

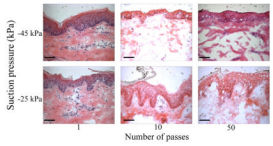

Figure 9.
Skin abraded using the dynamic mode microdermabrasion at −25 and −45 kPa suction pressure at 4.5 turns of the crystal flow rate knob applied for 1, 10, and 50 passes. Representative H&E-stained sections of porcine cadaver skin are shown. Scale bar = 50 μm.

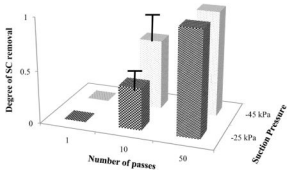

Figure 10.

Degree of stratum corneum removal during dynamic mode microdermabrasion at −25 and −45 kPa suction pressure at 4.5 turns of the crystal flow rate knob applied for 1, 10, and 50 turns. Complete stratum corneum removal = 1, partial stratum corneum removal = 0.5, and stratum corneum not removed = 0. Data represent the average of three replicate measurements ± standard deviation.

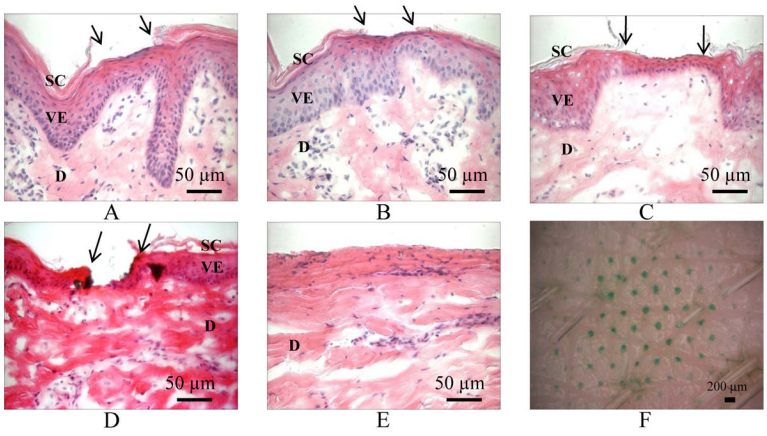

Figure 11.

Skin abraded using a mask containing 125 µm-diameter holes at −50 kPa suction pressure and the maximum crystal flow rate (0 turns) for 45 s (A), 60 s (B) and 90 s (C). (D) Skin abraded using a mask containing 250 µm-diameter holes at −50 kPa suction pressure at the maximum crystal flow rate for 30 s. The arrows point to sites of SC removal. (E) Skin abraded at the same condition as (A) without the mask; both the SC and VE were removed. (F) Skin abraded at the same condition as (B) imaged en face at lower magnification to show the holes stained with green dye. SC = stratum corneum, VE = viable epidermis, and D = dermis.

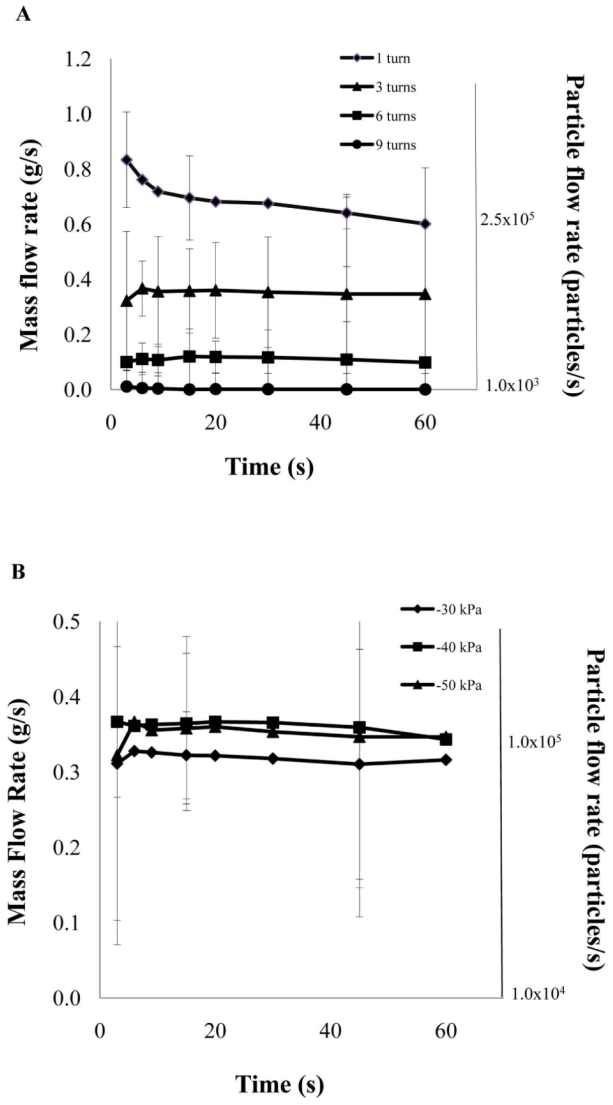

Figure A1.

Crystal mass flow rate and particle flow rate shown as a function of time at different crystal knob turns and suction pressures. (A) Mass and particle flow rates at 1, 3, 6, and 9 knob turns at a suction pressure of −50 kPa in the static mode. (B) Mass and particle flow rate at suction pressures of −30, −40, and − 50 kPa at a crystal flow rate at 3 turns in the static mode. Data represent the average of three replicate measurements ± standard deviation.

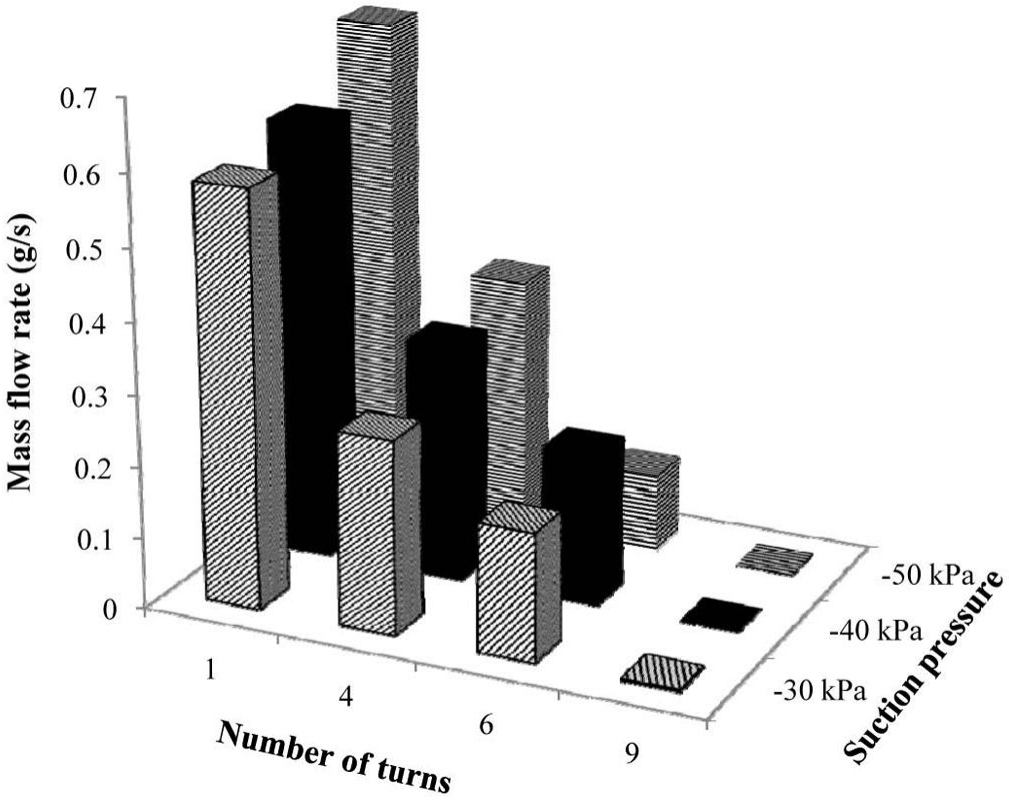

Figure A2.

Mass flow rate is shown as a function of suction pressure and number of turns of the crystal flow rate knob applied in the static mode. Data represent the average of three replicate measurements. Error bars are not shown to simplify the presentation. The magnitude of the error bars in these data is similar to those shown in Figure A1.

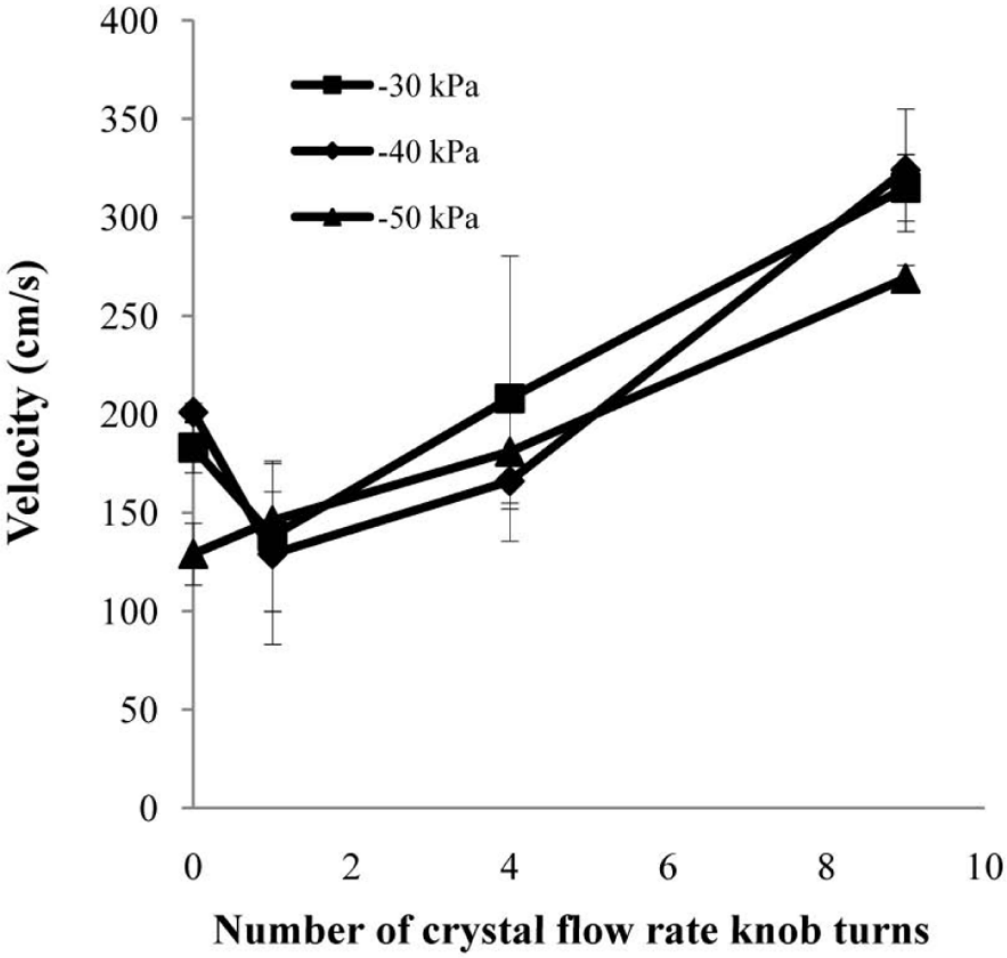

Figure A3.
Average crystal particle velocity shown as a function of the number of turns of the crystal flow rate knob at different suction pressures. Data represent the average of 20 particle measurements ± standard deviation.